European Journal of Pharmacology 951 (2023) 175786

Contents lists available at ScienceDirect

European Journal of Pharmacology

journal homepage: www.elsevier.com/locate/ejphar

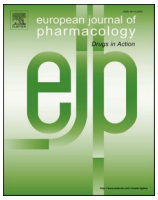

Dynamin-independent $Ca_V1.2$ and $K_{Ca}1.1$ channels regulation and vascular tone modulation by the mitochondrial fission inhibitors dynasore and dyngo-4a

Amer Ahmed [a,1], Alfonso Trezza [b], Mariangela Gentile [a], Eugenio Paccagnini [a], Alice Panti [a], Pietro Lupetti [a], Ottavia Spiga [b], Sergio Bova [c], Fabio Fusi [b,*]

[a] Dipartimento di Scienze della Vita, Università di Siena, via A. Moro 2, 53100, Siena, Italy
[b] Dipartimento di Biotecnologie, Chimica e Farmacia, Università di Siena, via A. Moro 2, 53100, Siena, Italy
[c] Department of Pharmaceutical and Pharmacological Sciences, University of Padova, Padova, Italy

ARTICLE INFO

Keywords:
Dynasore
Dyngo-4a
Mitochondrial fission
$Ca_V1.2$ channels
$K_{Ca}1.1$ channels
Molecular dynamic simulations

ABSTRACT

A role for mitochondrial fission in vascular contraction has been proposed based on the vasorelaxant activity of the dynamin (and mitochondrial fission) inhibitors mdivi-1 and dynasore. However, mdivi-1 is capable to inhibit Ba^{2+} currents through $Ca_V1.2$ channels ($I_{Ba1.2}$), stimulate $K_{Ca}1.1$ channel currents ($I_{KCa1.1}$), and modulate pathways key to the maintenance of vessel active tone in a dynamin-independent manner. Using a multidisciplinary approach, the present study demonstrates that dynasore, like mdivi-1, is a bi-functional vasodilator, blocking $I_{Ba1.2}$ and stimulating $I_{KCa1.1}$ in rat tail artery myocytes, as well as promoting relaxation of rat aorta rings pre-contracted by either high K^+ or phenylephrine. Conversely, its analogue dyngo-4a, though inhibiting mitochondrial fission triggered by phenylephrine and stimulating $I_{KCa1.1}$, did not affect $I_{Ba1.2}$ but potentiated both high K^+- and phenylephrine-induced contractions. Docking and molecular dynamics simulations identified the molecular basis supporting the different activity of dynasore and dyngo-4a at $Ca_V1.2$ and $K_{Ca}1.1$ channels. Mitotempol only partially counteracted the effects of dynasore and dyngo-4a on phenylephrine-induced tone. In conclusion, the present data, along with previous observations (Ahmed et al., 2022) rise caution for the use of dynasore, mdivi-1, and dyngo-4a as tools to investigate the role of mitochondrial fission in vascular contraction: to this end, a selective dynamin inhibitor and/or a different experimental approach are needed.

1. Introduction

Mitochondria are intracellular organelles that, beyond energy production, play a fundamental role in many other biological processes crucial for cell survival (Hoppins et al., 2020). In several tissues, they operate as an organised network navigating the cytoplasm, characterised by continuous cycles of fusion and fission, the so-called mitochondrial dynamics. Hallmarks of fission and fusion are fragmented or elongated/hyperconnected networks, respectively. Preserving a steady-state balance of fission-fusion rates is critical for both mitochondrial and cellular functions. This balance can be affected by changes in metabolism, signalling pathways, cell state, as well as pharmacological tools.

In general, cells metabolically active show increased mitochondrial dynamics: this allows rapid responses to various stimuli (Lisowski et al., 2018). However, mitochondrial fission and fusion seem to play a role also in pathological conditions, such as ischemia-reperfusion injury (Maneechote et al., 2017), neurodegenerative diseases (Reddy, 2014), and type 2 diabetes mellitus (Rovira-Llopis et al., 2017).

Progress in understanding the mechanism of action of the different dynamin superfamily GTPases that catalyse the constant fission and fusion of the mitochondrial networks (Ramachandran, 2018) has benefited from the discovery of inhibitors preventing the recruitment of dynamin to plasma membranes, including the GTPase inhibitors of

Abbreviations: $I_{Ba1.2}$, Ba^{2+} current through $Ca_V1.2$ channels; $I_{KCa1.1}$, K^+ current through $K_{Ca}1.1$ channels; KHS, modified Krebs-Henseleit solution; PF, pore-forming.

* Corresponding author.
E-mail address: fabio.fusi@unisi.it (F. Fusi).
[1] Present address: Department of Bioscience, Biotechnology and Environment, University of Bari, Via Edoardo Orabona, 70125 Bari, Italy.

https://doi.org/10.1016/j.ejphar.2023.175786
Received 2 January 2023; Received in revised form 3 May 2023; Accepted 10 May 2023
Available online 11 May 2023

dynamin-1 mdivi-1 (Lackner and Nunnari, 2010) and dynasore (Macia et al., 2006). The undesirable properties of dynasore, e.g., binding to serum proteins and detergents, later, led to the synthesis of the more potent analogue dyngo-4a (McCluskey et al., 2013). However, these commonly used inhibitors of dynamin and endocytosis show off-target, dynamin-independent effects, e.g., they are potent suppressors of mTORC1 activation (Persaud et al., 2018) and robustly inhibit fluid-phase endocytosis and peripheral membrane ruffling in engineered dynamin 1, 2, and 3 triple knockout fibroblasts (Park et al., 2013).

Dynasore and mdivi-1 are effective in animal models of diseases associated with altered mitochondrial dynamics (see References above). To our knowledge, however, no data in this context are available for dyngo-4a, which has been predominantly used to inhibit clathrin-dependent endocytosis *in vitro* (McCluskey et al., 2013). Dynasore and mdivi-1 have been assessed in rat aorta and mesenteric arteries to investigate the role of mitochondrial dynamics in the development of vascular smooth muscle contraction. Both agents relaxed phenylephrine-, endothelin 1-, and KCl-induced contractions by inhibiting mitochondrial fission; as a result, a role for mitochondrial dynamics in vessel contraction was proposed (Liu et al., 2016; Chen et al., 2017). However, this hypothesis has been recently argued by a multi-disciplinary study demonstrating that mdivi-1 inhibits also $Ca_V1.2$ channels, Ca^{2+} release from IP_3-sensitive Ca^{2+} store sites, and the Rho-A pathway as well as stimulates $K_{Ca}1.1$ channels, in a dynamin-independent manner (Ahmed et al., 2022), features that can by themselves support its vasorelaxant activity. Due to these "secondary effects", mdivi-1 seems not an adequate pharmacological tool to clarify whether mitochondrial fission is a required phenomenon for vascular smooth muscle contraction to occur. Therefore, in the present study, dynasore and dyngo-4a (Fig. 1) were evaluated as potential, selective candidate inhibitors of mitochondrial fission in vascular smooth muscle. To this end, a comparable multi-disciplinary approach was used to study their effects on vascular $Ca_V1.2$ and $K_{Ca}1.1$ channel function, on vessel mechanics, as well as their interaction *in silico* with channel protein residues. Results suggest that dynasore, displaying a similar profile to mdivi-1, does not possess a satisfactory selectivity as a dynamin inhibitor and, therefore, its use to dissect the functional interplay between mitochondrial fission and vascular smooth muscle contraction is not recommended. Further experiments are needed to clarify whether dyngo-4a, behaving differently from its analogue, may be considered selective.

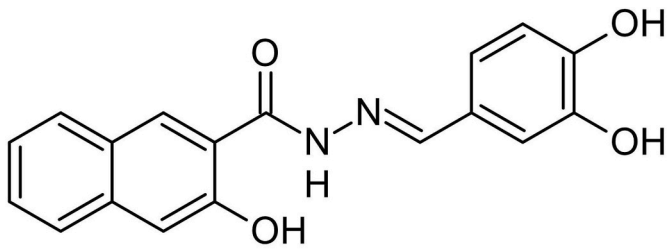

dynasore

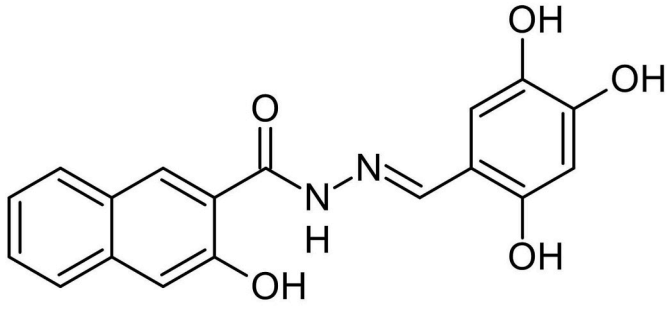

dyngo-4a

Fig. 1. Molecular structures of the dynamin modulators.

2. Materials and methods

2.1. Animal care statement

Male Wistar rats (250–350 g; Charles River Italia, Calco, Italy) were anaesthetized with isoflurane (4%) and O_2 gas mixture using Fluovac (Harvard Apparatus, Holliston, Massachusetts, USA), before decapitation and exsanguination. The tail main artery and abdominal aorta were rapidly removed and immersed in the external solution and modified Krebs-Henseleit solution (KHS; see below for composition), respectively, and processed as detailed below.

2.2. Cell isolation procedure

Smooth muscle cells, previously characterised in depth (see Mugnai et al., 2014), were dissociated from an 8-mm long piece of the tail main artery incubated at 37 °C for 35–45 min in 2 mL of external solution containing 0.1 mM Ca^{2+}, 20 mM taurine (equally balanced with NaCl), 1.1 mg/mL collagenase (type XI), 1 mg/mL soybean trypsin inhibitor, and 1 mg/mL BSA, bubbled with carboxygen (95% O_2–5% CO_2) (Budriesi et al., 2009). External solution (in mM): 130 NaCl, 5.6 KCl, 10 HEPES, 20 glucose, 1.2 $MgCl_2$, and 5 Na-pyruvate; pH 7.4. The cell suspension, stored in 0.05 mM Ca^{2+}, 20 mM taurine, and 0.5 mg/mL BSA external solution at 4 °C, was used for a maximum of two days (Mugnai et al., 2014).

2.3. Whole-cell patch-clamp recordings

The conventional whole-cell configuration of the patch-clamp technique was used to record Ba^{2+} currents through $Ca_V1.2$ channels ($I_{Ba1.2}$) and K^+ currents through $K_{Ca1.1}$ channels ($I_{KCa1.1}$). Borosilicate glass recording electrodes (WPI, Berlin, Germany) had a pipette resistance of 2–4 MΩ. An Axopatch 200B patch-clamp amplifier (Molecular Devices Corporation, Sunnyvale, CA, USA) applied voltage pulses to single tail artery myocytes and recorded the corresponding membrane currents. The junction potential, whole-cell capacitance, and series resistance (between 70% and 75%) were compensated. Low-pass filtered (1 kHz) current signals, recorded at 20–22 °C, were digitized at 3 kHz (Fusi et al., 2002). A peristaltic pump (LKB 2132, Bromma, Sweden) was used to superfuse (flow rate of 400 μl/min) cells.

2.4. $I_{Ba1.2}$ recordings

Single myocytes were initially superfused with a 0.1 mM Ca^{2+} and 30 mM tetraethylammonium external solution. The internal solution contained (in mM) 100 CsCl, 10 HEPES, 11 EGTA, 2 $MgCl_2$, 1 $CaCl_2$ (free Ca^{2+} concentration pCa 8.4), 5 Na pyruvate, 5 succinic acid, 5 oxaloacetic acid, 3 Na_2ATP, and 5 phosphocreatine (pH 7.4 with CsOH). $I_{Ba1.2}$, elicited with 250-ms clamp pulses (0.067 Hz) to 10 mV from a V_h of −50 mV and recorded in 30 mM tetraethylammonium and 5 mM Ba^{2+} external solution, stabilized in 7–10 min after the whole-cell configuration had been obtained, and did not run down for at least 40 min (Fusi et al., 2008). Tetraethylammonium and Cs^+, in the external and internal solution, respectively, blocked K^+ currents, whereas 10 μM nifedipine, completely blocking $I_{Ba1.2}$, allowed leakage and residual inward or outward currents subtraction offline. The external solution containing 30 mM tetraethylammonium and 5 mM Ba^{2+}, and the internal solution had an osmolarity of 320 mosmol and 290 mosmol, respectively (as measured by an Osmostat OM 6020 osmometer, Menarini Diagnostics, Florence, Italy).

2.5. $I_{KCa1.1}$ recordings

$I_{KCa1.1}$ was recorded using an external solution (containing, in mM: 145 NaCl, 6 KCl, 10 glucose, 10 HEPES, 5 Na-pyruvate, 1.2 $MgCl_2$, 0.1 $CaCl_2$, 0.003 nicardipine; pH 7.4) and an internal solution (containing in mM: 90 KCl, 10 NaCl, 10 HEPES, 10 EGTA, 1 $MgCl_2$, 6.41 $CaCl_2$; free Ca^{2+} concentration pCa 7.0; pH 7.4) with an osmolarity of 310 mosmol and 265 mosmol, respectively (as measured by an Osmostat OM 6020 osmometer, Menarini Diagnostics, Florence, Italy). $I_{KCa1.1}$, recorded for 500 ms from a V_h of −40 mV to avoid voltage-dependent K^+ channels activation, stabilized in about 6–10 min and remained stable for the following 20–30 min [Iozzi et al. (2013). Tetraethylammonium (1 mM), proved to be a specific blocker of $K_{Ca}1.1$ channels at this concentration (Tykocki et al., 2017), was added at the end of each experiment to allow current correction for leakage (offline).

2.6. Aorta ring preparation

Rings (3 mm wide) were cut from the abdominal aorta and mounted, under a passive tension of 1 g, in organ baths, filled with KHS (composition in mM: 118 NaCl, 4.75 KCl, 1.19 KH_2PO_4, 1.19 $MgSO_4$, 25 $NaHCO_3$, 11.5 glucose, 2.5 $CaCl_2$, gassed with carboxygen; pH 7.4) for isometric tension recordings using a digital PowerLab data acquisition system (PowerLab 8/30; ADInstruments, Castle Hill, Australia). After a 60-min equilibration period, ring viability was accomplished by measuring the response to both 0.3 μM phenylephrine (pharmaco-mechanical coupling) and 60 mM KCl (electro-mechanical coupling). The endothelium was removed by gently rubbing the lumen of the ring with a forceps tip. The absence of a functional endothelium was proved by the lack of response to the addition of 10 μM acetylcholine at the plateau of phenylephrine-induced contraction (Fusi et al., 2000).

2.7. Functional experiments

Cumulative concentrations of dynasore or dyngo-4a were added to aorta rings stimulated either by 0.3 μM phenylephrine or high KCl concentrations [25 mM or 60 mM KCl; Cuong et al., 2014). In some experiments, rings were pre-incubated with 10–80 μM dyngo-4a before constructing a concentration-response curve to either KCl or phenylephrine. Nifedipine (1 μM) and/or sodium nitroprusside (100 μM) was added at the end of each experiment to test the viability of smooth muscle.

To analyse the effects of dynasore and dyngo-4a on Ca^{2+} release from intracellular stores and extracellular Ca^{2+} influx triggered by phenylephrine, rings were pre-incubated with each compound or vehicle (DMSO), first for 30 min in normal KHS, and then for 5 min in a Ca^{2+}-free KHS containing 1 mM EGTA. The subsequent addition of 10 μM phenylephrine (this maximal concentration was required to obtain a measurable contraction in the absence of extracellular Ca^{2+}) evoked a contraction representing the release of Ca^{2+} from the sarcoplasmic reticulum. The following addition of 3.5 mM Ca^{2+} caused a further contraction due to the influx of extracellular Ca^{2+} (Fusi et al., 2015). Responses were measured as a percentage of the contraction induced by 60 mM KCl in KHS.

2.8. Transmission electron microscopy

Rings (1.5-mm wide) were pre-incubated with vehicle (DMSO) or 80 μM dyngo-4a for 20 min before stimulation with 0.3 μM phenylephrine or left untreated in the organ bath (control). Then the preparations were unmounted, rinsed 4 times in 0.1 M sodium cacodylate buffer (pH 7.2) and fixed in 2.5% glutaraldehyde diluted in cacodylate buffer for 3 h at 4 °C, washed in cacodylate buffer overnight, and then post-fixed in 1% osmium tetroxide for 1 h at 4 °C. Following an additional rinse in cacodylate buffer, samples were dehydrated with a graded series of ethanol and embedded in Epon epoxy resin, positioning the samples to obtain cross-sections. Aortic vessel 70-nm thin sections, prepared with a Reichert Ultracut E ultramicrotome (Reichert-Jung AG, Wien, Austria) and collected on 150 mesh copper grids, were routinely stained with uranyl acetate and lead citrate and observed with an FEI Tecnai G2 Spirit transmission electron microscope (FEI Company, Hillsboro, OR, USA) at an electron accelerating voltage of 120 kV, equipped with a TVIPS TemCam-F216 CMOS camera (TVIPS GmbH, Gauting, Germany). Images of the samples were acquired at 6800X and later the mitochondria were manually measured using ImageJ software (ver 1.53j, NIH, http://imagej.nih.gov/ij/), taking into account the following parameters: aspect ratio (major axis/minor axis) and roundness [4 x area/(π x major axis^2)].

2.9. In silico methods

The *Rattus norvegicus* $Ca_V1.2$ channel α_{1C} subunit and $K_{Ca}1.1$ channel 3D structures were obtained through a homology modelling procedure as previously described (Trezza et al., 2022; Ahmed et al., 2022). The 3D structures of dynasore and dyngo-4a (compound CID: 135533054 and 136227923, respectively) were downloaded in sdf format using the PubChem database (Kim et al., 2019). OpenBabel tool (O'Boyle et al., 2011) generated and converted the structure in a pdbqt 3D format adding gasteiger partial charge. Dock Prep application (Pettersen et al., 2004) optimized the structure before the docking procedure, while the MGLTOOLS script (Morris et al., 2009) converted in pdbqt format the 3D model structures, as previously described (Fusi et al., 2016; Teodori et al., 2019). To identify the potential binding pose of compounds on $Ca_V1.2$ and $K_{Ca}1.1$ channels, a docking simulation was performed with Autodock/VinaXB (Koebel et al., 2016), building a box of 14x15x10 Å and 10x15x10 Å for the X, Y, and Z dimensions, respectively, enclosing all binding pocket residues; the other parameters were set by default. The interaction profile was analysed by P.L.I.P. software using all parameter settings by default (Salentin et al., 2015). To propose a potential mechanism of action, a classical molecular dynamics simulation of 100 ns was performed for the $Ca_V1.2$ channel 3D model bound to compounds, as previously described (Trezza et al., 2022). GROMACS 2019.3 was used to carry out the classical molecular dynamics simulations, while molecular dynamics trajectories were analysed by GROMACS 2019.3 package using all parameter settings by default (Berendsen et al., 1995). PyMOL v2.5 was used as Molecular Graphics System to generate Figures (The PyMOL Molecular Graphics System, Version 2.5, Schrödinger, LLC).

2.10. Materials

The chemicals used were: acetylcholine, BSA, collagenase (type XI), dyngo-4a, nifedipine, phenylephrine, taurine, tetraethylammonium chloride, and soybean trypsin inhibitor (Sigma Chimica, Milan, Italy); sodium nitroprusside (Riedel-De Haen AG, Seelze Hannover, Germany); dynasore and mito-tempol (Abcam, Milan, Italy); sodium cacodylate, (Acros organics Geel, Belgium); glutaraldehyde and osmium tetroxide (Ted Pella, Inc. Redding, CA, USA); Epon epoxy resin (Serva Electrophoresis GmbH, Heidelberg, Germany); uranyl acetate (Fluka Chemie AG, Buchs, Switzerland); and lead citrate (Carlo Erba Reagents Srl, Cornaredo, Milan, Italy). Phenylephrine was solubilized in 0.1 M HCl, nifedipine in ethanol, dynasore and dyngo-4a in DMSO, mito-tempol in distilled water. Neither DMSO nor ethanol (maximal concentration of 0.1%, v/v) affected vascular responses (data not shown).

2.11. Statistical analysis

LabChart 7.3.7 Pro (PowerLab; ADInstruments, Castle Hill, Australia), pCLAMP 9.2.1.8 (Molecular Devices Corporation, Sunnyvale, CA, USA), and GraphPad Prism 5.04 (GraphPad Software Inc.) performed the analysis of data, which are reported as mean ± SD; n is the number of rings or cells analysed (indicated in parentheses), isolated from at least three animals. GraphPad Prism 5.04 (GraphPad Software

Inc.) performed the statistical analysis by one-way or repeated measures ANOVA (followed by Dunnett post-hoc test) or Student's *t*-test for either paired or unpaired samples (two-tailed). $P < 0.05$ was considered significant. Nonlinear regression analysis provided pIC_{50} or pEC_{50} values and E_{max} values, i.e., drug potency and efficacy, respectively.

3. Results

3.1. Dynasore but not dyngo-4a inhibits $I_{Ba1.2}$

The effect of dynasore was studied on $I_{Ba1.2}$, elicited with a clamp pulse to 10 mV from a V_h of −50 mV (0.067 Hz), recorded in single rat tail artery myocytes. As shown in Fig. 2, dynasore caused a marked, though slow, concentration-dependent inhibition of peak $I_{Ba1.2}$ (Fig. 2A and B).

Dynasore (80 μM) reduced $I_{Ba1.2}$ amplitude elicited with various depolarising steps (from −30 mV to 50 mV) without modifying the voltage-dependence of the current (Fig. 2C).

To investigate whether dynamin inhibition was responsible for the Ca^{2+} antagonistic activity of dynasore, a different modulator (namely the inhibitor dyngo-4a) was studied. When myocytes were challenged with 80 μM dyngo-4a (0.38 μM being required to inhibit dynamin-1 by 50%; McCluskey et al., 2013), the current amplitude was similar to that recorded under control conditions (Fig. 2D). Dyngo-4a did not modify the current-voltage relationship (data not shown).

A biophysical analysis of the effect of the two dynamin inhibitors on $I_{Ba1.2}$ kinetics was performed. Dynasore and dyngo-4a prolonged the activation time constant, but only the former significantly prolonged also the inactivation one (Fig. 3).

3.2. Dynasore inhibits whereas dyngo-4a potentiates KCl-induced contraction

The effect of dynasore on electromechanical coupling was assessed in rings depolarized by high KCl concentrations. Cumulative addition of the compound caused concentration-dependent relaxation of aorta preparations depolarized by either 25 mM or 60 mM KCl with pIC_{50} values of 5.61 ± 0.56 (n = 7) and 4.19 ± 0.29 (n = 5; P = 0.0005), respectively (Fig. 4A). In contrast to dynasore, its analogue dyngo-4a caused an increase in vessel tone induced by 60 mM KCl that seemed to be concentration-dependent (Fig. 4A). Furthermore, it was capable to raise basal tone under control conditions (Fig. 4B) and trigger muscle contraction in rings depolarized by moderate concentrations of KCl (i.e., 25 mM; Fig. 4C). Noticeably, the latter effect was not antagonized by the presence of 100 nM prazosin in the organ bath. However, due to the great variability in the response to dyngo-4a (the maximum values ranged from 48.1% to 157.4% of the contraction induced by 60 mM KCl), the pEC_{50} value could not be calculated; those estimated from the average curve were 5.59 and 5.54, respectively. Finally, dyngo-4a significantly potentiated the response of the preparations to

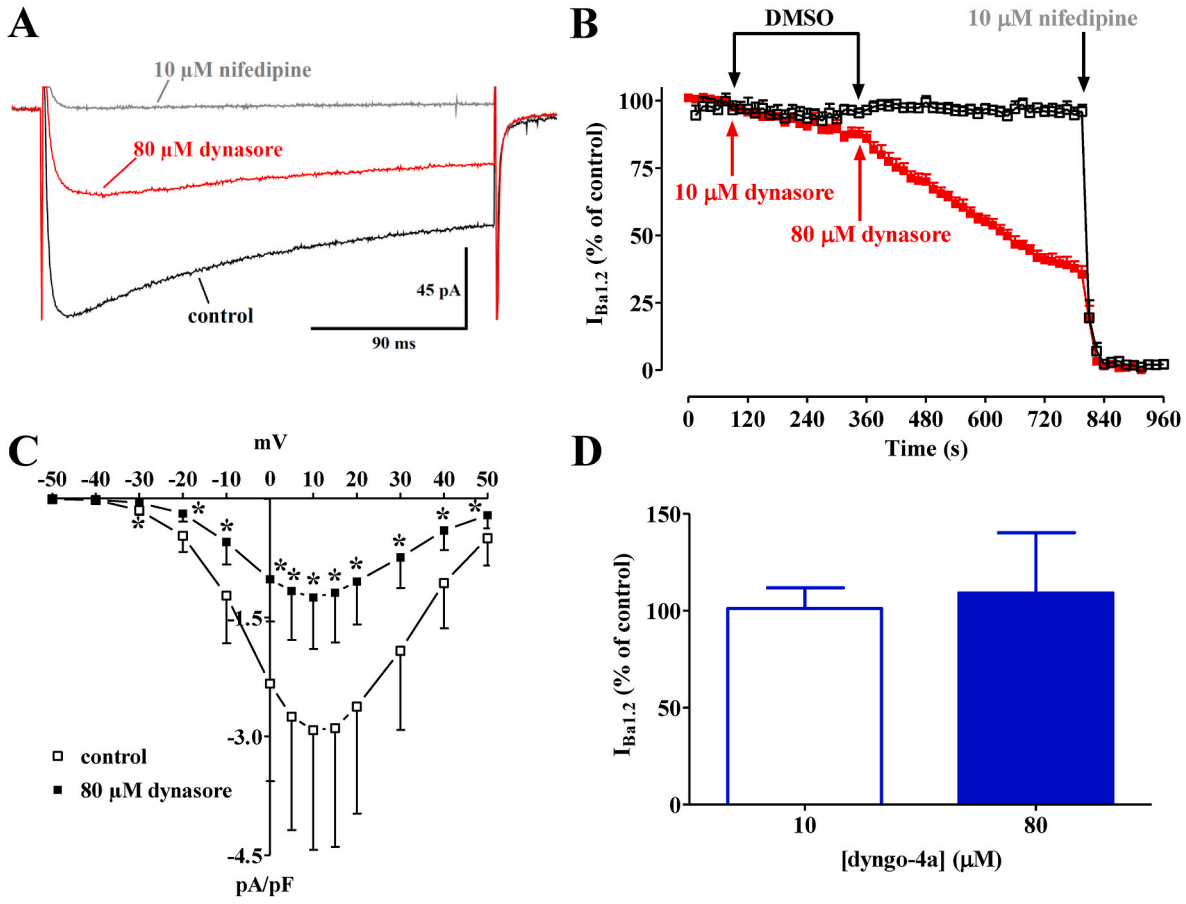

Fig. 2. Effects of dynasore and dyngo-4a on $I_{Ba1.2}$ in single rat tail artery myocytes. (A) Traces of $I_{Ba1.2}$, averaged from 6 cells, evoked by 250-ms clamp pulses to 10 mV from a V_h of −50 mV, recorded under control conditions or in the presence of 80 μM dynasore. The effect of 10 μM nifedipine is also shown. (B) Time course of $I_{Ba1.2}$ inhibition caused by dynasore. Currents were recorded at a frequency of 0.067 Hz (every 15 s) and subsequently normalized to the amplitude recorded just before the addition of the first concentration of dynasore (indicated by the arrows). Nifedipine (10 μM) suppressed $I_{Ba1.2}$. Data points are the mean ± SD (n = 6). (C) Current-voltage relationships, recorded from V_h of −50 mV, constructed in the absence (control) or presence of 80 μM dynasore. Currents measured during the various test pulses are plotted against the membrane potential and expressed as pA/pF. Data points are mean ± SD (n = 6). *P < 0.05 vs control, Student's t-test for paired samples (two-tailed). (D) Effects of dyngo-4a on $I_{Ba1.2}$. Columns are the mean ± SD (n = 5).

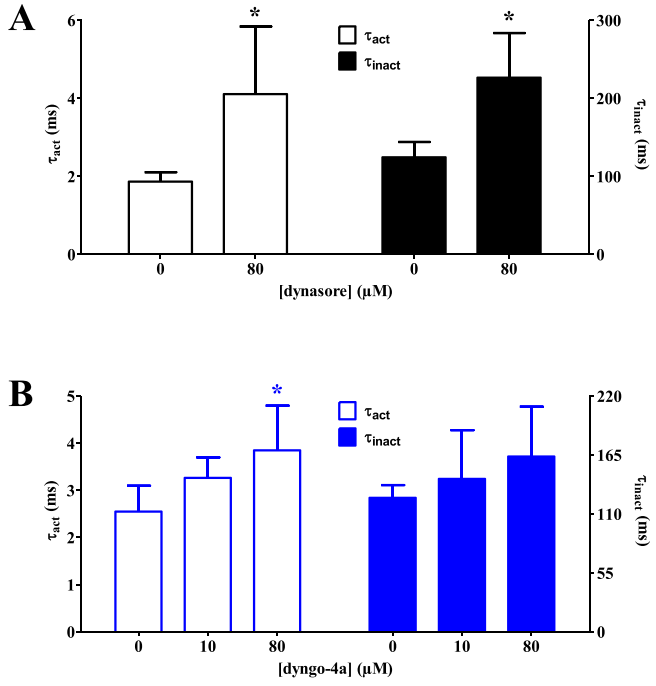

Fig. 3. Effect of dynasore and dyngo-4a on $I_{Ba1.2}$ kinetics in single rat tail artery myocytes. The time constant for activation (τ_{act}) and inactivation (τ_{inact}) were measured in the absence or presence of various concentrations of (A) dynasore or (B) dyngo-4a. Columns represent the mean ± SD (n = 5–6). *P < 0.05 vs control (0), Student's *t*-test for paired samples or repeated measures ANOVA and Dunnett post-test.

cumulative concentrations of KCl (pEC_{50} values of 1.55 ± 0.06 1.4 mM DMSO, 1.68 ± 0.06 10 μM dyngo-4a, n = 5; P = 0.0086; 1.58 ± 0.07 11.2 mM DMSO, 1.82 ± 0.13 80 μM dyngo-4a, n = 5; P = 0.0063; Fig. 4D).

3.3. Dynasore inhibits whereas dyngo-4a potentiates phenylephrine-induced contraction: role of mitochondria-derived radicals

As a previous report (Liu et al., 2016) showed that, in rat mesenteric arteries, phenylephrine-induced contraction is mediated by mitochondria-derived radicals, the effect of the mitochondrial-targeted antioxidant mito-tempol was assessed on the phenylephrine-induced contraction of aorta rings. As shown in Fig. 5A, pre-incubation of endothelium-denuded rings with 10 μM mito-tempol moderately reduced the response to the selective α_1 receptor agonist (pEC_{50} values of 6.46 ± 0.44 control, n = 14, and 6.38 ± 0.46 mito-tempol, n = 14, respectively; P = 0.6314). Dynasore, when added cumulatively to preparations pre-contracted by 0.3 μM phenylephrine, caused a concentration-dependent relaxation (pIC_{50} value of 5.04 ± 0.28, n = 6; Fig. 5B) that was counteracted by mito-tempol though only at the maximum dynasore concentration assessed (pIC_{50} value of 4.73 ± 0.30, n = 14; P = 0.0979). In rings pre-incubated with 10 μM dyngo-4a, potency (pEC_{50} values of 6.40 ± 0.52 DMSO, n = 8; 7.21 ± 0.16 dyngo-4a, n = 7; P < 0.05) and efficacy of phenylephrine significantly increased (Fig. 5C). When also 10 μM mito-tempol was present, the phenylephrine concentration-response curve was still significantly shifted to the left (7.04 ± 0.13 dyngo-4a + mito-tempol, n = 7; P < 0.05) while the E_{max} was similar to that recorded under control conditions.

In another series of experiments, the effect of dynasore and dyngo-4a were assessed on Ca^{2+} release from intracellular store sites and Ca^{2+} influx from the extracellular environment triggered by phenylephrine. Both Ca^{2+} release (measured as muscle tension triggered by phenylephrine in the absence of extracellular Ca^{2+}) and Ca^{2+} influx triggered by the α_1 receptor agonist were significantly reduced by 80 μM dynasore (Fig. 5D). However, pre-treatment with 10 μM dyngo-4a increased, though not significantly, both responses to phenylephrine.

3.4. Dynasore and dyngo-4a stimulate $I_{KCa1.1}$

The relaxant activity of dynasore became less pronounced as the extracellular K^+ concentration was raised, a behaviour distinctive of K^+ channel opener; therefore, its effect on iberiotoxin-sensitive $I_{KCa1.1}$ was studied (Saponara et al., 2006). The addition of 10 μM dynasore did not modify the current amplitude (Fig. 6A). However, when drug concentration was raised to 80 μM, a striking (about 500% of control at 70 mV) and significant stimulation of $I_{KCa1.1}$ was observed in the range of membrane potential 20–70 mV (Fig. 6A and B). Surprisingly, also the analogue, vasoconstricting dyngo-4a stimulated $I_{KCa1.1}$, though its efficacy was only around 170% of control (Fig. 6C and D).

3.5. Dynasore and dyngo-4a dock to $Ca_V1.2$ and $K_{Ca}1.1$ channels

The potential binding poses of the dynamin inhibitors on the *Rattus norvegicus* $Ca_V1.2$ channel α_{1C} subunit and $K_{Ca}1.1$ channel homology models were predicted through a docking simulation. The best-docked conformations of dynasore and dyngo-4a showed Gibbs free-energy values (ΔG) for the $Ca_V1.2$ channel of −6.1 kcal mol^{-1} and -7.0 kcal mol^{-1}, while for the $K_{Ca}1.1$ channel of −5.0 kcal mol^{-1} and -4.6 kcal mol^{-1}, respectively. In the $Ca_V1.2$ channel, both compounds were positioned between the S6-III and S6-IV segments, close to the central pore (Fig. 7A). The interaction network analysed by the P.L.I.P. tool demonstrated that dynasore formed a hydrophobic interaction with Ala-1183C (S6-III), a hydrogen bond with Ser-1141 (pore-forming; PF), and a parallel π-stacking with Phe-1143C (PF) (Fig. 7B). Similarly, dyngo-4a triggered hydrophobic interactions with Phe-778B (cytoplasmatic), Phe-1143C (PF), and Ala-1183C (S6-III), along with three hydrogen bonds with Gln-1069C (S5-III), Ser-1141C (PF) and Tyr-1178C (S6-III) (Fig. 7C).

To confirm the protein structural integrity, and the binding pose stability of the inhibitors, and to propose a potential mechanism of action, a classical molecular dynamics simulation of 100 ns was performed on the backbone of the $Ca_V1.2$ channel in complex with dynasore and dyngo-4a. Both radius of gyration (around 2.18 nm for dynasore and 2.15 nm for dyngo-4a) and root mean square deviation (around 0.22 nm and 0.31 nm, respectively) showed a stable trend during the whole run (Fig. 7D). The binding poses of dynasore and dyngo-4a exhibited an average root mean square deviation value of 0.1 nm and 0.2 nm, respectively.

The gmx distance function implemented in GROMACS 2019.3, used to evaluate the lifetime of the π-stacking interaction between the naphthalene-composing phenyl ring of the 2-naphthol group of dynasore and dyngo-4a with the phenyl ring of Phe-1143C, showed a distance average of 0.28 nm and 0.7 nm, respectively (Fig. 7E).

The strength of the interaction energy of compounds with the $Ca_V1.2$ channel during the classical molecular dynamics simulation run was computed by the gmx energy function implemented in GROMACS 2019.3. The non-bonded interaction energy of dynasore and dyngo-4a for the α_{1C} subunit was −403.22 ± 6.9 kJ mol^{-1} (corresponding to −98.3 ± 1.7 kcal mol^{-1}) and −142.53 ± 6.2 kJ mol^{-1} (corresponding to −34.7 ± 0.3 kcal mol^{-1}), respectively.

While dynasore docked in a cytoplasmic region of the $K_{Ca}1.1$ channel (Fig. 8B), giving rise to three hydrophobic interactions with Phe-457C, Lys-458C, and Phe-461C, along with two hydrogen bonds with Glu-440C and Phe-466C, dyngo-4a formed a wide hydrophobic and polar interaction network. The P.L.I.P. analyses showed four hydrophobic interactions with Tyr-398C, Phe-457C, Phe-461C, and Phe-466C, along with seven hydrogen bonds with Lys-164B, Asn-238B, Glu-440C, Thr-462C, Val-464C, Glu-465C, and Phe-466C (Fig. 8C).

Unfortunately, due to the low cover value of the $K_{Ca}1.1$ channel

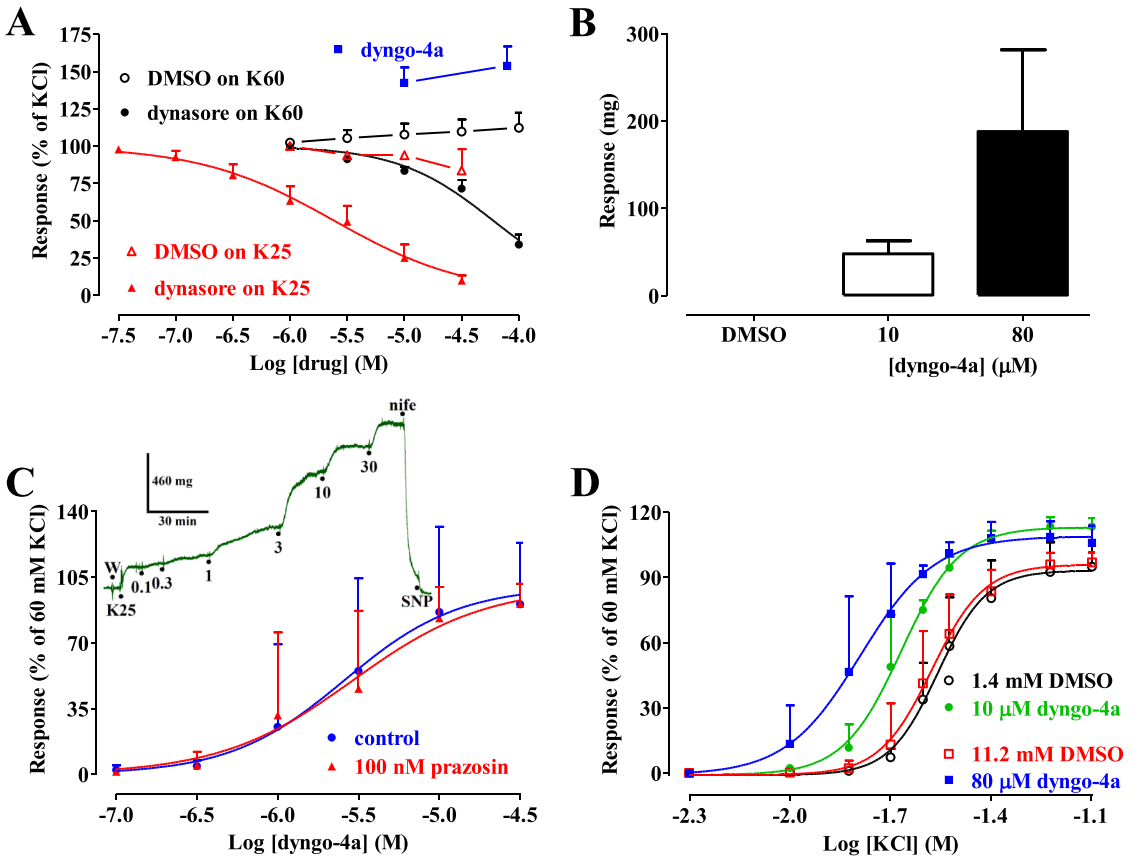

Fig. 4. Effect of dynasore and dyngo-4a on depolarized rat aorta rings. (A) Endothelium-denuded preparations were stimulated by 60 mM (K60) or 25/30 mM KCl (K25), and then either dynasore or dyngo-4a was added cumulatively. In the ordinate scale, the response is reported as a percentage of the initial contraction induced by KCl. Data points represent the mean ± SD (n = 4–7). (B) Effect of dyngo-4a on ring basal tone. Contraction is expressed in mg. Columns represent the mean ± SD (n = 5). (C) Effect of dyngo-4a on rings depolarized by a moderate concentration of KCl. Rings were stimulated by 25 mM KCl, in the absence (control) or presence of 100 nM prazosin, before the addition of cumulative concentrations of dyngo-4a. Data points are the mean ± SD (n = 5–10). In the ordinate scale, the response is reported as a percentage of the contraction induced by 60 mM KCl in ring functional assay. Inset: trace (representative of 9 experiments) of tension developed in response to dyngo-4a at the indicated concentrations (μM). The preparation was bathed in KHS containing 25 mM KCl (K25). The effect of 10 μM nifedipine (nife) and 100 μM sodium nitroprusside (SNP) is also shown. W: wash. (D) Effect of dyngo-4a on the contraction elicited by high KCl. Concentration-response curves to KCl were constructed in presence of various concentrations of dyngo-4a or DMSO. Data points are the mean ± SD (n = 5) and represent the percentage of the contraction induced by 60 mM KCl in ring functional assay.

against the template in some protein regions and the low confidence of their secondary structure prediction, the structural integrity of the channel during the classical molecular dynamics run ensued altered and could not be performed.

3.6. Dynasore and dyngo-4a antagonise phenylephrine-induced mitochondrial fission

The effects of phenylephrine, dynasore and dyngo-4a on mitochondrial fission were evaluated in rat aorta ring *tunica media* myocytes. Comparative morphometry accomplished by transmission electron microscopy imaging demonstrated that in control rings mitochondria showed the physiologic, canonical elongated strip shape and scattered distribution (Fig. 9A). In rings challenged by 0.3 μM phenylephrine and vehicle alone, mitochondria were short, round, and clustered (Fig. 9B). However, when rings were pre-incubated with either 80 μM dyngo-4a or 80 μM dynasore, mitochondria showed the same morphometry as that observed in control samples (Fig. 9C–D). Statistical analyses of the mitochondrial fission morphometry parameters confirmed the above ultrastructural analyses (Fig. 9E–F).

4. Discussion

One of the key findings of this work is the striking divergence between dynasore and dyngo-4a vascular activity. While dynasore inhibited $I_{Ba1.2}$, stimulated $I_{KCa1.1}$, and showed a prominent spasmolytic effect on electro- and both components (extracellular and intracellular) of the pharmaco-mechanical coupling, dyngo-4a displayed vasoconstricting properties, as it not only increased muscle passive tone but also markedly potentiated high KCl- and phenylephrine-induced contractions. This observation was even more surprising when considering the remarkable similarity of their structures (dyngo-4a being characterised by the presence of only an additional OH group on the phenolic ring) as well as the comparable inhibition of mitochondrial fission.

The mechanisms underlying the different vasoactivity of the dynamin modulators were explored analysing their effects on two of the main pathways underpinning vessel tone regulation, namely $Ca_V1.2$ and $K_{Ca}1.1$ channels. The electrophysiology data clearly demonstrated that dynasore is a $Ca_V1.2$ channel blocker, inhibition being concentration-dependent. $Ca_V1.2$ channel blockade is in line with the relaxant effect of this agent on high KCl-induced contraction, which is essentially due to the opening of these channels and the consequent influx of extracellular Ca^{2+}. Noticeably, the dynamin inhibitor caused a delay in the transition between the resting and the activated states as well as between the

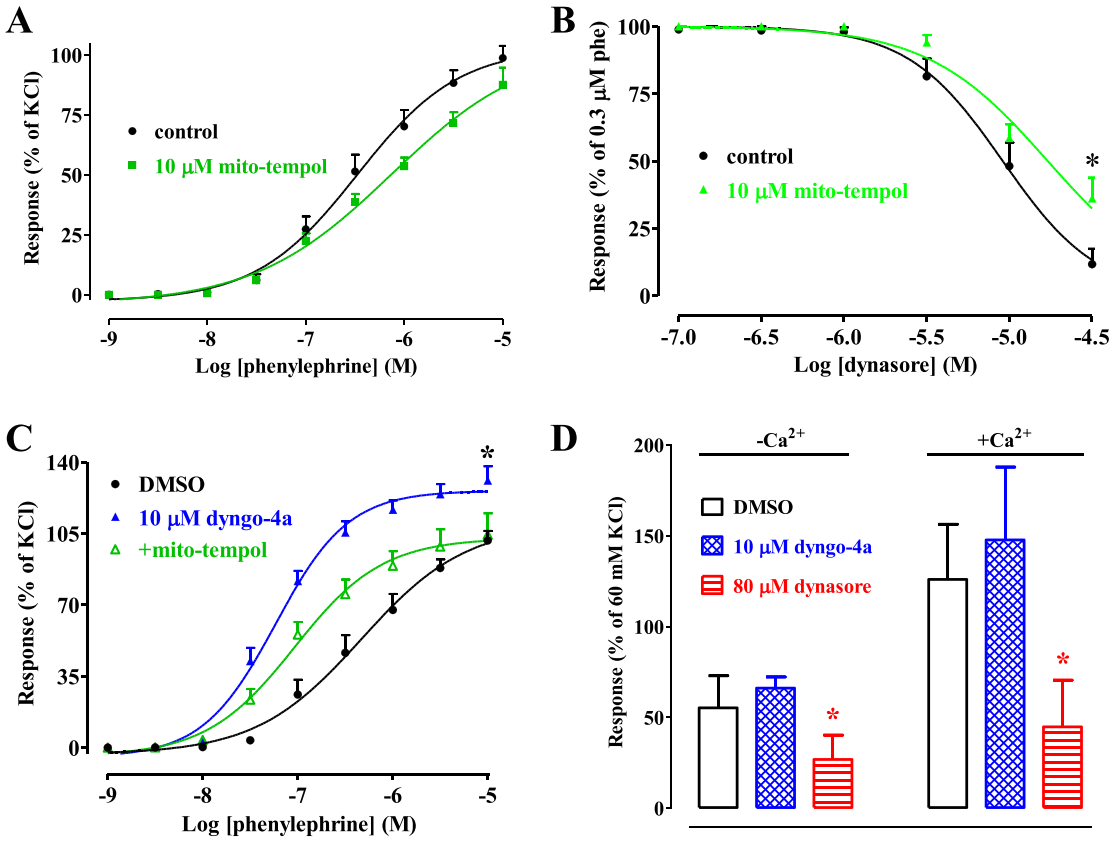

Fig. 5. Effect of mito-tempol, dynasore, and dyngo-4a on phenylephrine-induced contraction of rat aorta rings. (A) Endothelium-denuded preparations were stimulated by cumulative concentrations of phenylephrine, either in the absence or presence of 10 μM mito-tempol. Data points are the mean ± SD (n = 14) and represent the percentage of the contraction induced by 60 mM KCl in ring functional assay. (B) Dynasore concentration-response curves constructed in aorta rings pre-contracted by 0.3 μM phenylephrine, either in the absence or presence of 10 μM mito-tempol. Data points are the mean ± SD (n = 6) and represent the percentage of the contraction induced by the α_1 receptor agonist. *P = 0.0282, Student's t-test for unpaired samples (two-tailed). (C) Phenylephrine concentration-response curves constructed in aorta rings pre-incubated with vehicle (DMSO), 10 μM dyngo-4a or drug plus 10 μM mito-tempol. Data points are the mean ± SD (n = 6–8) and represent the percentage of the contraction induced by 60 mM KCl in ring functional assay. *P < 0.05 vs. DMSO, one-way ANOVA and Dunnett's post-test. (D) Effects of dynasore and dyngo-4a on Ca^{2+} release from intracellular stores and on extracellular Ca^{2+} influx induced by phenylephrine in endothelium-denuded rings. Effect of vehicle only (11.3 mM DMSO), 10 μM dyngo-4a or 80 μM dynasore on 10 μM phenylephrine-induced contraction in the absence (-Ca^{2+}) and presence of extracellular Ca^{2+} (+Ca^{2+}). Contractions were measured independently, the response to phenylephrine in the absence of extracellular Ca^{2+} representing the baseline for that obtained after the addition of extracellular Ca^{2+}. Columns are the mean ± SD and represent the percentage of the response to 60 mM KCl in ring functional assay. *P < 0.05 vs. DMSO, one-way ANOVA and Dunnett's post-test.

activated and the inactivated states of the channel. Surprisingly, these features are distinctive of $Ca_V1.2$ channel stimulators like Bay K 8644 and quercetin (Saponara et al., 2002; Saponara et al., 2008) but different from those of nifedipine, verapamil, and diltiazem (representative of the dihydropyridine, phenylalkylamine, and benzothiazepine classes of Ca^{2+} antagonists), which accelerate the inactivation kinetics leaving unaltered that of activation (McDonald et al., 1994). Dynamin seemed not involved in $Ca_V1.2$ channel blockade because the more potent inhibitor dyngo-4a did not affect $I_{Ba1.2}$ amplitude, though it slowed down the transition of the channel from the resting to the activated state.

Docking simulation results showed that both dynasore and dyngo-4a docked close to the surface of the $Ca_V1.2$ channel pore between domains III and IV of the S6, a binding region for channel modulators (Zhao et al., 2019), sharing a similar binding pose. This is not surprising, given the striking similarity of their structures. Either molecule triggered several interactions within the target binding pocket. Interestingly, the comparison of the interaction network by the P.L.I.P. tool of the $Ca_V1.2$ channel and dynasore or dyngo-4a complexes with the rabbit $Ca_V1.1$--verapamil complex (i.e., a homologue biological system in complex with a Ca^{2+} antagonist; Protein Data Bank code: 6JPA), and the rabbit $Ca_V1.1$-Bay K 8644 complex (i.e., in complex with a $Ca_V1.2$ channel agonist; Protein Data Bank code: 6JP8; Zhao et al., 2019) demonstrated that the two dynamin inhibitors, albeit sharing an extremely similar binding pose and region, formed key interactions either with Phe-1143C (corresponding to Phe-1013 of the rabbit $Ca_V1.1$ channel) or with Gln-1069C (corresponding to Gln-939 of the rabbit $Ca_V1.1$ channel), which are residues crucial for the activity of the channel (Zhao et al., 2019; Trezza et al., 2022; Ahmed et al., 2022). Noticeably, dyngo-4a, similarly to Bay K 8644, triggered a hydrogen bond between the hydroxyl group in C1 of the 1,3,4-trihydroxy-benzene moiety and the nitrogen of the Gln-1069C side chain, which prevented any interaction with Phe-1143C. Conversely, this hydrogen bond was not triggered by dynasore that, similarly to verapamil, moved to Phe-1143C and formed a π-stacking between its naphthalene-composing phenyl ring of the 2-naphthol group and the phenyl ring of the residue. However, only mutagenesis experiments can support and strengthen this hypothesis.

The molecular dynamics simulation confirmed the docking simulation results. The RMSD and Rg profiles of the protein backbone of the $Ca_V1.2$ channel in complex with either molecule showed high stability during the run, excluding the presence of artifacts in the simulations. Despite their similar binding pose, dynasore exhibited considerable binding stability and non-bonded interaction energy, higher than dyngo-

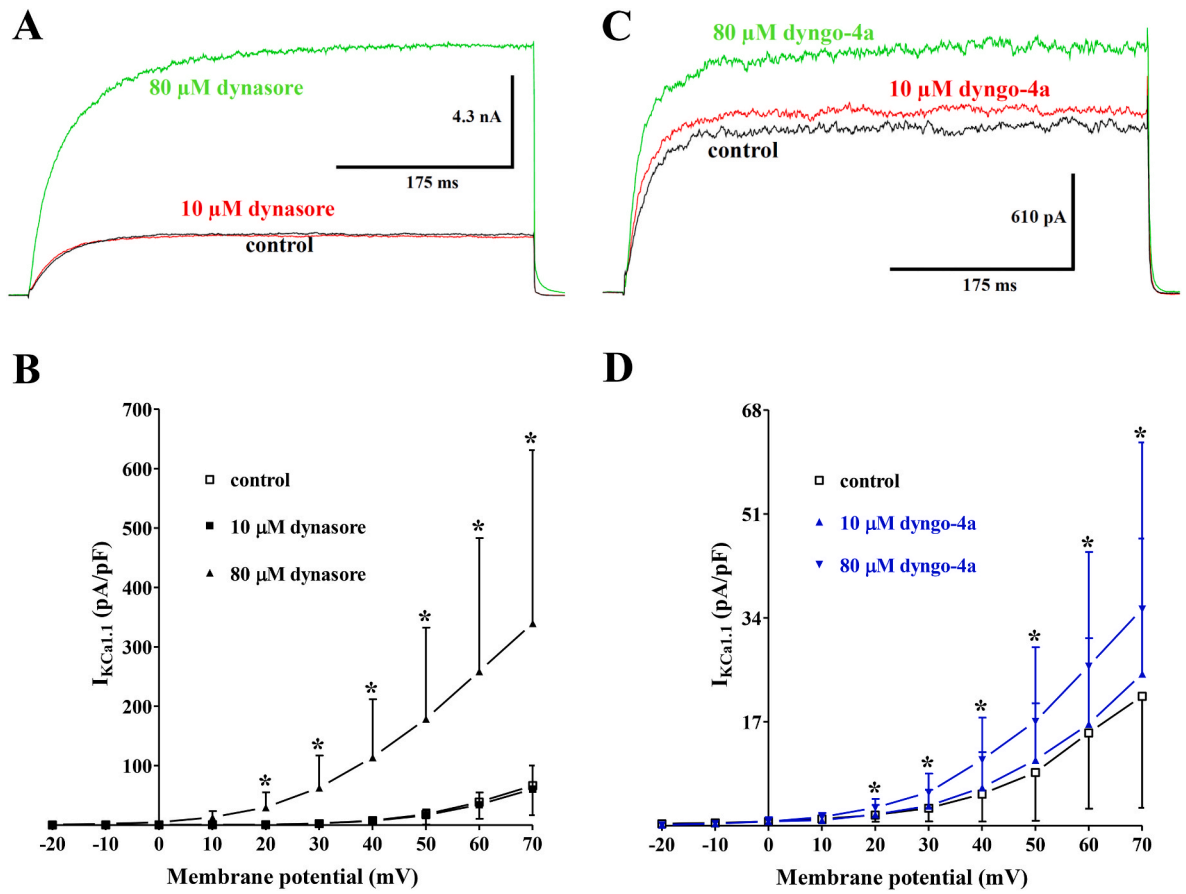

Fig. 6. Effects of dynasore and dyngo-4a on $I_{KCa1.1}$ in single tail artery myocytes. (A,C) Original recordings (average traces of 5 and 8 cells, respectively) of conventional whole-cell $I_{KCa1.1}$ elicited by a 500 ms voltage step from V_h −40 to 70 mV, measured in the absence (control) and presence of 10 μM and 80 μM (A) dynasore or (C) dyngo-4a. (B,D) Current-voltage relationships obtained before the addition (control) and in the presence of various concentrations of either (B) dynasore or (D) dyngo-4a. On the ordinate scale, the response is reported as current density in pA/pF. Data points are the mean ± SD. *P < 0.05 vs. control, repeated measures ANOVA and Dunnett's post-test.

4a. Furthermore, the average distance of the quinazoline-composing phenyl ring of the 2-mercapto-quinazolin-4(3H)-one group of dynasore and the side chain of Phe-1143C key residue demonstrated that the parallel π-stacking was maintained for the entire run, suggesting the ability of dynasore to alter the biological function of the channel. Taken together, these results are consistent with the hypothesis that dynasore inhibition of $Ca_V1.2$ channels is attained through strong and specific interactions with the channel protein and provide a reasonable explanation for the different vascular activity that characterises dynasore and dyngo 4a.

In addition to the $Ca_V1.2$ channel blocking activity, dynasore caused a marked increase in current amplitude through the $K_{Ca}1.1$ channel, which is in line with the relaxant effect exerted by the drug on rings depolarized by moderate concentrations of KCl. Under these experimental conditions, in fact, K^+ channel openers are effective vasodilators because their muscle relaxant activity is directly correlated to the transmembrane chemical gradient for K^+ (Gurney, 1994): the larger the difference (e.g., in the presence of 25 mM extracellular KCl as opposed to 60 mM KCl), the greater the efflux of K^+ through the open channels (leading to membrane hyperpolarization and $Ca_V1.2$ channels closure) and the higher the vasodilation. Likewise, dyngo-4a stimulated $I_{KCa1.1}$; however, the magnitude of the effect was lower than that brought about by dynasore. This suggested that the presence of an additional OH group in the phenolic ring of dynasore, not only abolished the Ca^{2+} antagonistic effect but had also a marked impact on the $K_{Ca}1.1$ channel stimulatory activity.

The docking analysis demonstrated that both dynasore and dyngo-4a docked in a $K_{Ca}1.1$ channel sensing region close to the S6/RCK linker with a high binding affinity (Gessner et al., 2012), triggering several hydrophobic and polar interactions. Interestingly, both molecules formed a hydrophobic interaction with Lys-458C and Tyr-398C, respectively, and shared the interaction with Phe-461C. In a previous study, these residues were identified as potential key targets for the binding to, and biological function of the $K_{Ca}1.1$ channel (Carullo et al., 2020). These data, though consistent with the hypothesis that $I_{KCa1.1}$ stimulation induced by dynasore and dyngo-4a is the result of the direct binding of the compounds to the channel protein, need to be validated through experimental mutagenesis. Noteworthy, dynasore and, more effectively, dyngo-4a increase TMEM175 lysosomal K^+ current of *Xenopus laevis* oocytes by increasing the number of channels in the plasma membrane, though a simultaneous stimulation of channel activity was not ruled out (Pergel et al., 2021). Therefore, it can be speculated that also an enhanced translocation of $K_{Ca}1.1$ channels to the plasma membrane of rat tail myocytes may contribute to the $I_{KCa1.1}$ stimulatory activity of dynasore and dyngo-4a.

An intriguing result of the present study is the vascular activity of dyngo-4a, observed under several, different experimental conditions. In fact, dyngo-4a, likewise the $Ca_V1.2$ channel agonist Bay K 8644 (Fusi et al., 2003), increased muscle tone under resting conditions as well as potentiated both phenylephrine- and KCl-induced contractions. This observation, along with the *in-silico* data discussed above, points to dyngo-4a as a direct activator of $Ca_V1.2$ channels. However, this hypothesis was not supported by the patch-clamp analysis. Furthermore, the vasoconstricting activity of dyngo-4a was not affected by the

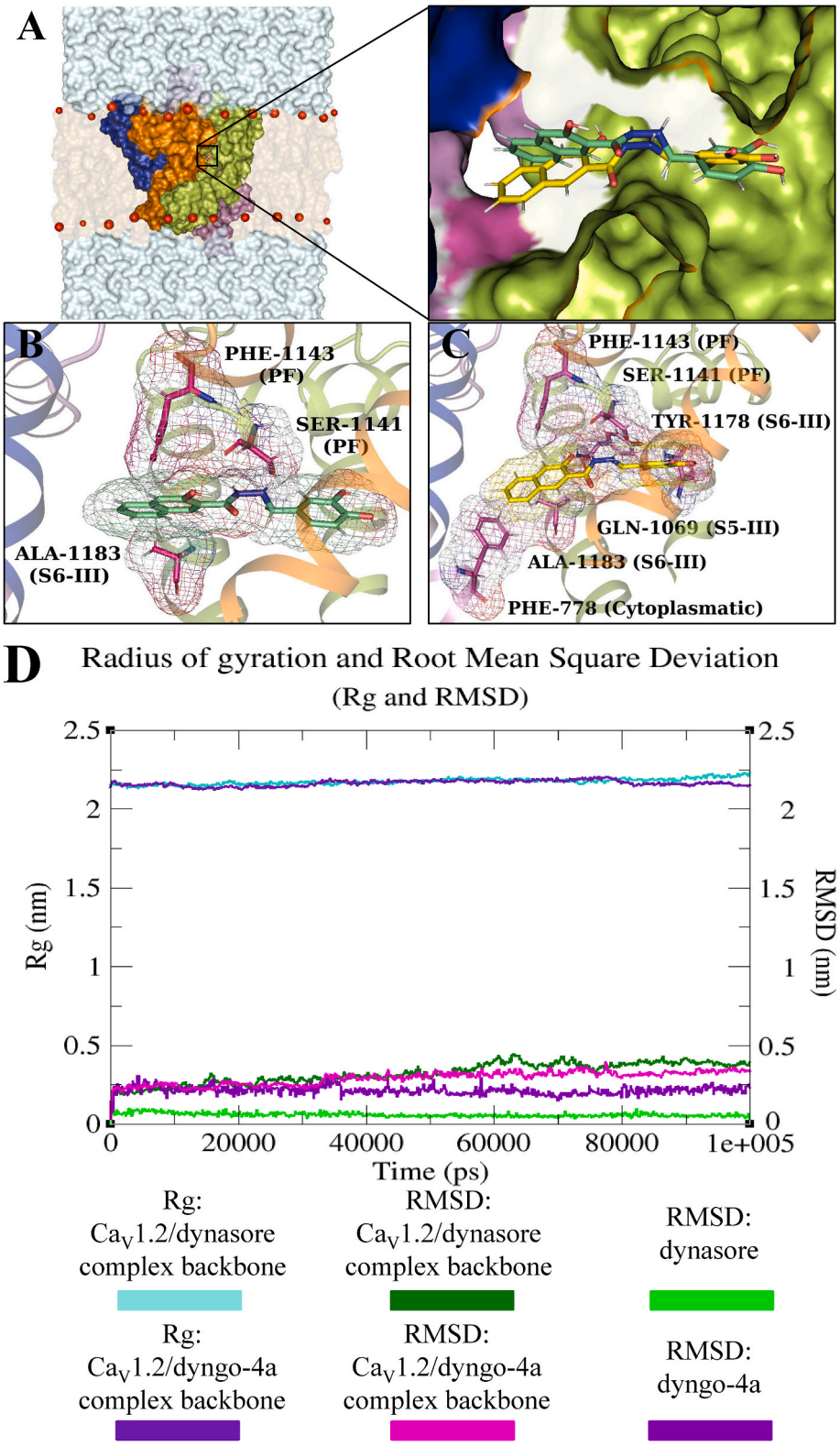

Fig. 7. Overview of $Ca_V1.2$ channel docked with dynasore and dyngo-4a. (A) The $Ca_V1.2$ channel 3D structure is depicted in a multicolour surface. The bilayer is illustrated as an orange transparent surface, while some phospholipid heads are reported in red spheres. The extracellular and cytoplasmic sides are shown as cyan transparent surfaces. Enlarged view of the docked poses of dynasore and dyngo-4a within the $Ca_V1.2$ channel binding pocket, whose surface is shown in cross-section. (B–C) Interaction network of (B) dynasore and (C) dyngo-4a in complex with the $Ca_V1.2$ channel after the docking simulation. (D) Radius of gyration (Rg) and Root Mean Square Deviation (RMSD) profiles of the $Ca_V1.2$ channel in complex with dynasore and dyngo-4a, depicted as coloured lines. Rg (nm) and RMSD (nm) are reported on the left and right Y-axis, respectively, and the time (ps) of the molecular dynamics run on the X-axis. (E) Distance average profiles (depicted as coloured lines) between the $Ca_V1.2$ channel Phe-1143C side-chain and the naphthalene-composing phenyl ring of the 2-naphthol group of dynasore and dyngo-4a. Rg (nm) and RMSD (nm) are reported on the left and right Y-axis, respectively, and the time (ps) of the molecular dynamics run on the X-axis.

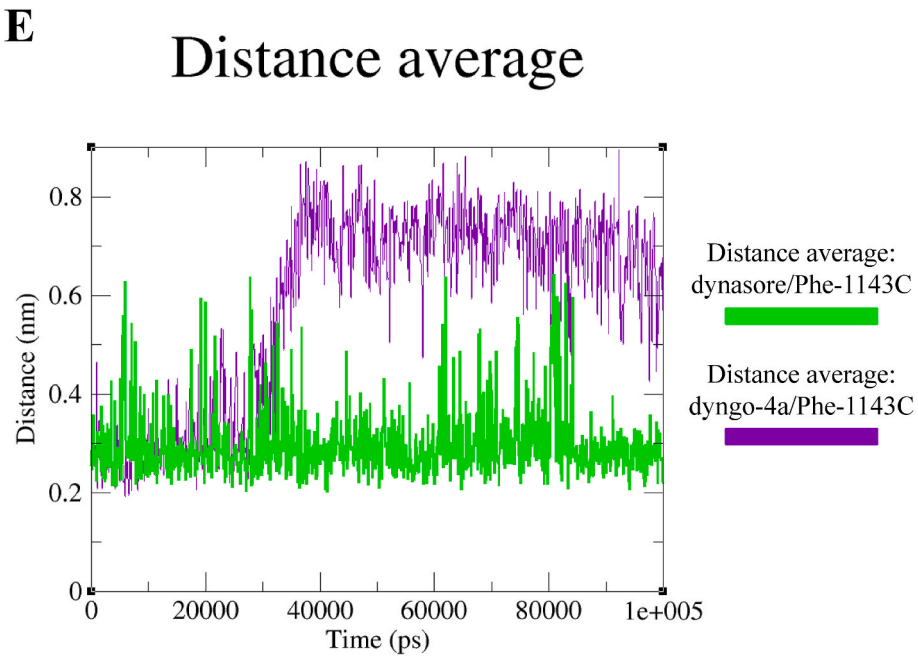

Fig. 7. (*continued*).

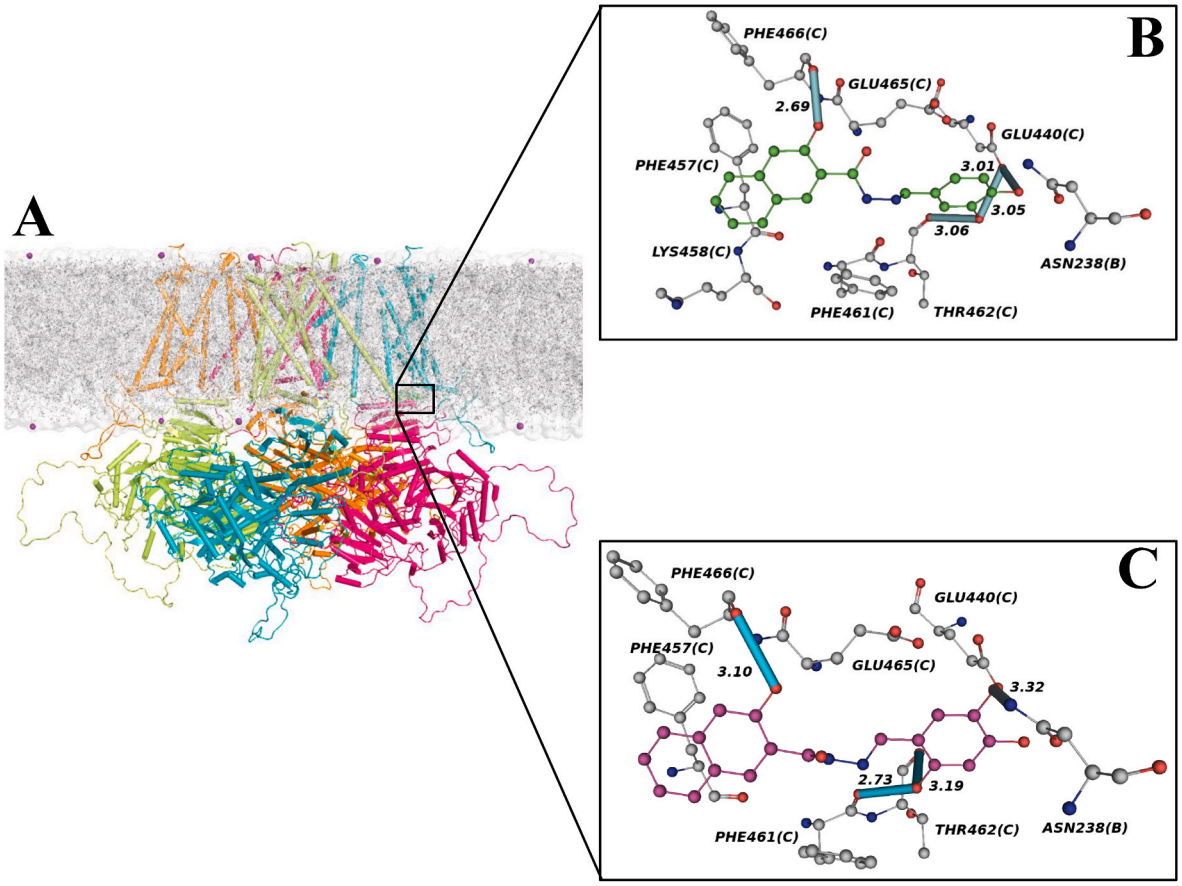

Fig. 8. Overview of the $K_{Ca}1.1$ channel docked with dynasore and dyngo-4a. (A) The $K_{Ca}1.1$ channel 3D structure is depicted in multicolour cartoon. The bilayer is illustrated as a grey transparent surface and lines, while some phospholipid heads are depicted as purple spheres. (B,C) Interaction network of (B) dynasore and (C) dyngo-4a in complex with the $K_{Ca}1.1$ channel after the docking simulation. The binding residues are shown in grey balls and sticks, while dynasore and dyngo-4a are displayed as green and purple balls and sticks, respectively. Hydrogen bonds are depicted as cyan cylinders, with numbers indicating the bond length (Å).

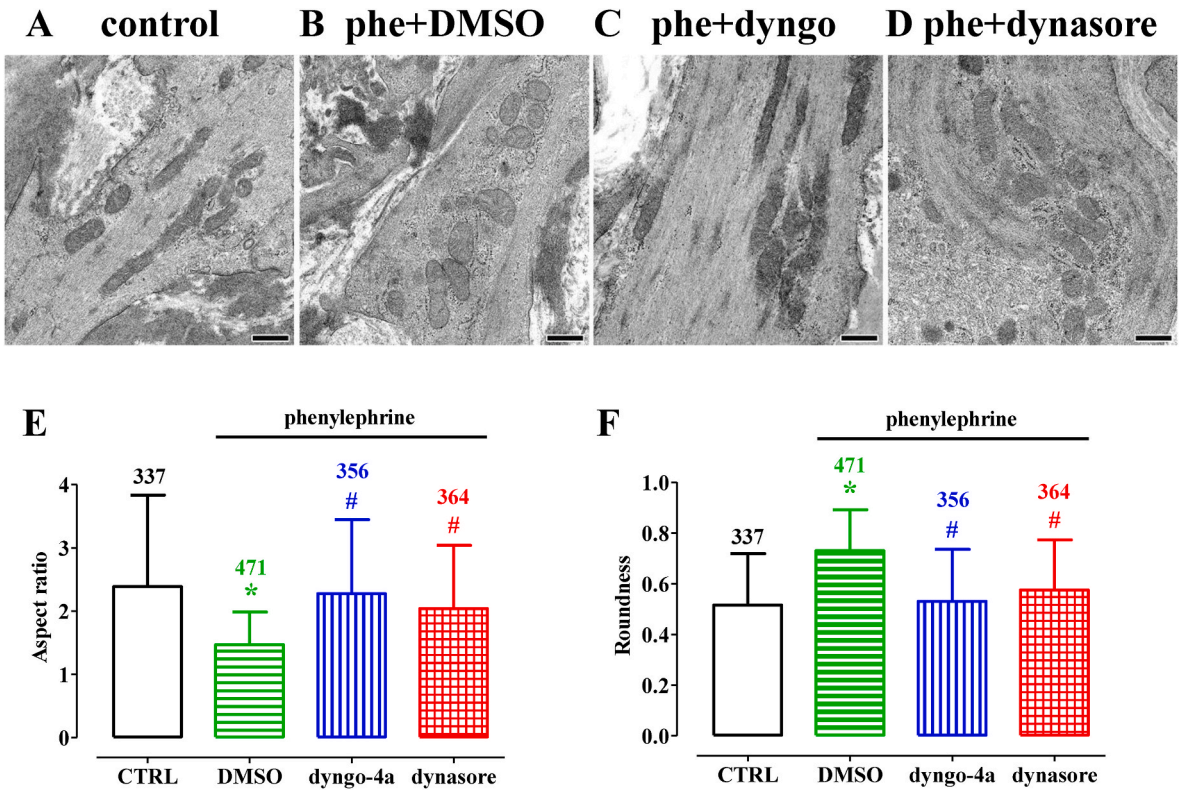

Fig. 9. Effect of dynasore and dyngo-4a on phenylephrine-induced mitochondrial fission. (A–D) Transmission electron microscope images captured in aorta rings (A) under control conditions, and pre-contracted by 0.3 μM phenylephrine in the presence of either (B) vehicle (DMSO), (C) 80 μM dyngo-4a or (D) 80 μM dynasore pre-incubated for 20 min (scale bar = 500 nm). (E–F) Summary of (E) aspect ratio and (F) roundness data representative of mitochondrial fission. Columns represent the mean ± SD, the numbers of mitochondria analysed per group being shown above the bars. *P < 0.05 vs control (CTRL), Student's t-test for unpaired samples (two-tailed); #P < 0.05 vs DMSO, one-way ANOVA and Dunnett's post-test.

presence of prazosin, a selective α_1 receptor antagonist, thus ruling out the possible involvement of a release of catecholamine from perivascular nerves triggered by the dynamin inhibitor. Therefore, further experiments are necessary to elucidate the mechanism(s) underpinning dyngo-4a vasoactivity that, however, goes beyond the scope of the present study.

Recently, Liu et al. (2016) hypothesized that vessel stimulation by various agents is followed by an increase in intracellular Ca^{2+} concentration, mitochondrial fission, and production of reactive oxygen species that, in turn, promote blood vessel contraction. Hence, mitochondrial fission inhibitors, such as dynasore and mdivi-1, may represent a novel class of vasorelaxant agents. However, this hypothesis has been argued by a recent multi-disciplinary study demonstrating that mdivi-1 is capable to target not only mitochondrial fission but also several pathways involved in the regulation of vessel tone (namely $Ca_V1.2$ and $K_{Ca}1.1$ channels, Ca^{2+} release from IP_3-sensitive Ca^{2+} store sites, and likely Rho-A kinase; Ahmed et al., 2022), thus leading to a concerted reduction of intracellular Ca^{2+} concentration. Therefore, it is likely that both vasorelaxation and inhibition of mitochondrial fission (which is a Ca^{2+}-dependent process; Hom et al., 2007; Hom et al., 2010) observed with mdivi-1 are in part or totally mediated by dynamin-independent mechanisms. The results of the present study, in which a similar multi-disciplinary approach was pursued, strongly support the latter hypothesis. In fact, they clearly show that also dynasore, which antagonises mitochondrial fission triggered by these vasoconstrictors (Liu et al., 2016; present paper), relaxed vascular smooth muscle by inhibiting $Ca_V1.2$ channels and stimulating $K_{Ca}1.1$ channels. Furthermore, and maybe more importantly, they demonstrate that dyngo-4a, a dynamin inhibitor structurally related to and more potent than dynasore (McCluskey et al., 2013), which did not affect $Ca_V1.2$ channels and weakly stimulated $K_{Ca}1.1$ channels, was unable to relax both phenylephrine- and KCl-induced contraction, though reverting mitochondrial fission triggered by these vasoconstrictors.

In rat mesenteric arteries, the mitochondria-targeted, radical scavenger mito-tempol abolished phenylephrine-induced constriction without affecting the associated mitochondrial fission (Liu et al., 2016). However, in aorta rings stimulated by the same α_1 receptor agonist, the effect of mito-tempol was weak and not significant (present paper), thus suggesting that mitochondrial-generated radicals may or may not play a role in mediating phenylephrine-induced vasoconstriction, depending on either the vessel type or the vasoconstrictor used (see Chen et al., 2017). Furthermore, mito-tempol significantly antagonized the effect of both dynasore and dyngo-4a, reducing the vasorelaxant efficacy of the former and the active tone potentiation of the latter, respectively. This observation suggests that mitochondrial radicals indeed contribute to the vascular effects of the two dynamin inhibitors; at present, the possibility that superoxide anions generated by the catechol moieties present in their structure cannot be ruled out. Further investigation, however, is required to clarify this issue, which goes beyond the scope of the present investigation.

In conclusion, the present data strengthen and broaden a previous hypothesis (Ahmed et al., 2022) rising caution for the use of the most popular dynamin modulators, namely dynasore and mdivi-1, in vascular smooth muscle studies, as their off-target activity might lead to misinterpretation of the results obtained. As mitochondrial dynamics is a Ca^{2+}-dependent process, in fact, they are not appropriate tools to discern the consequences of dynamin inhibition from those of intracellular Ca^{2+} concentration decrease on smooth muscle contractility (Fig. 10). Furthermore, also the supposed role of mitochondrial fission in the pathogenesis of neurodegenerative diseases (Reddy, 2014), ischemia-reperfusion injury (Maneechote et al., 2017), and type 2 diabetes mellitus (Rovira-Llopis et al., 2017), as hypothesized based on the

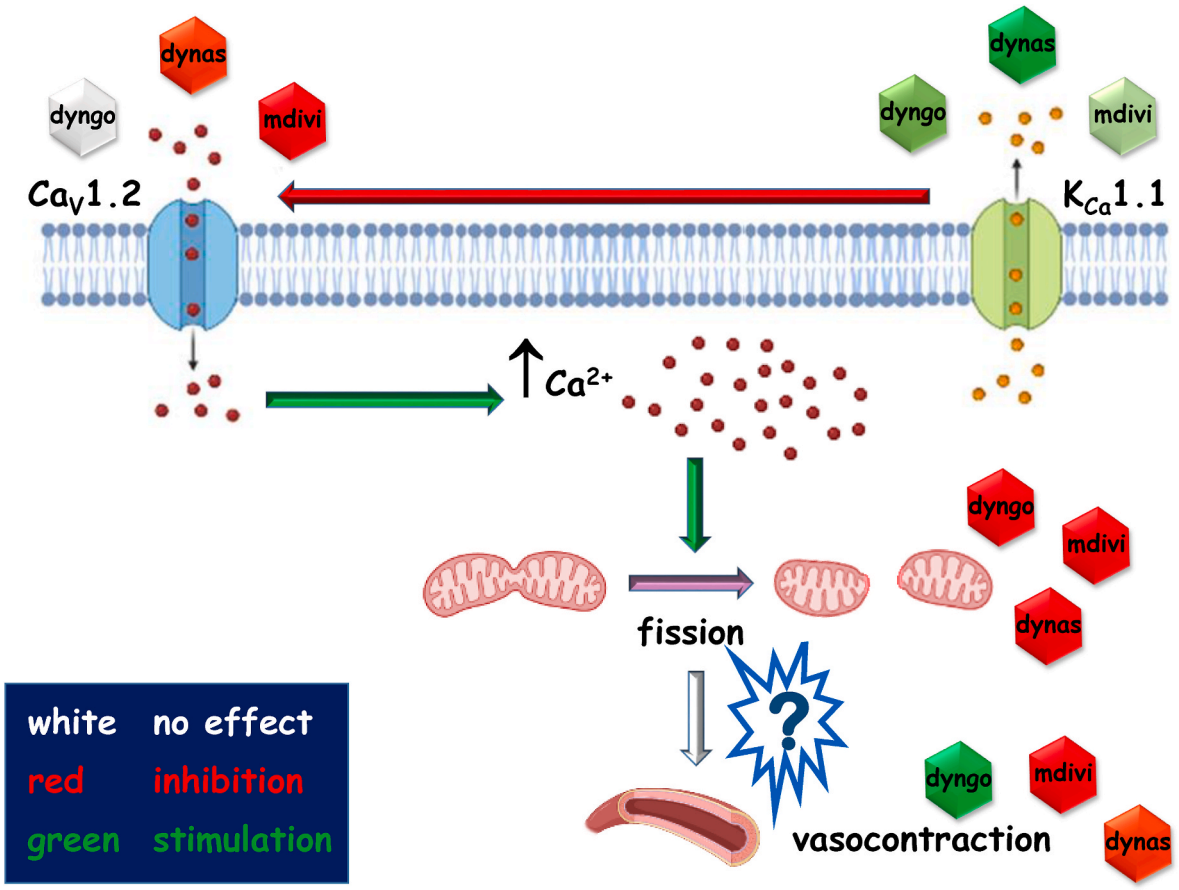

Fig. 10. Effects of mitochondrial fission inhibitors on vascular smooth muscle cells. Cartoon summarizing the results obtained in the present paper and Ahmed et al. (2022). Abbreviations: dyngo, dyngo-4a; dynas, dynasore; mdivi, mdivi-1. The darker the intensity of the green and red colours, the greater the effect (stimulation or inhibition, respectively).

beneficial effects of mdivi-1 and dynasore observed in these conditions, should be re-evaluated because also Ca^{2+} channel blockers exert the same protective effects (Vezzani et al., 1988; Jesmin et al., 2002; Simonovic et al., 2019). Finally, dyngo-4a seems to be a tool more selective than dynasore and mdivi-1, due to the lack of effect on $Ca_V1.2$ channels, consistent with new speculation that mitochondrial fission counteracts, rather than sustains, vascular smooth muscle contraction. However, a different experimental approach is necessary to understand whether mitochondrial fission, occurring during aorta smooth muscle contraction, is simply a "secondary effect" not crucial to or rather plays a role in muscle tone regulation.

Ethics statement

All the procedures were approved by the Animal Care and Ethics Committee of the University of Siena and the Italian Department of Health (7DF19.N.TBT), in strict accordance with the European Union Guidelines for the Care and the Use of Laboratory Animals (European Union Directive, 2010/63/EU).

Funding

Not applicable.

CRediT authorship contribution statement

Amer Ahmed: Investigation, Formal analysis. **Alfonso Trezza:** Investigation, Formal analysis, Writing – original draft. **Mariangela Gentile:** Investigation, Formal analysis. **Eugenio Paccagnini:** Investigation, Formal analysis. **Alice Panti:** Investigation, Formal analysis. **Pietro Lupetti:** Supervision, Writing – review & editing. **Ottavia Spiga:** Supervision. **Sergio Bova:** Conceptualization, Writing – review & editing, Supervision. **Fabio Fusi:** Conceptualization, Methodology, Investigation, Formal analysis, Writing – original draft, Writing – review & editing, Supervision.

Declaration of competing interest

The authors declare that they have no known competing financial interests or personal relationships that could have appeared to influence the work reported in this paper.

Data availability

Data will be made available on request.

Acknowledgements

We wish to thank Dr.s Dumi Marradi and Gioele Mancini for their assistance in some preliminary experiments, and Dr Paolo Fiorenzani for technical support.

References

Ahmed, A., Trezza, A., Gentile, M., Paccagnini, E., Lupetti, P., Spiga, O., Bova, S., Fusi, F., 2022. The drp-1-mediated mitochondrial fission inhibitor mdivi-1 impacts the function of ion channels and pathways underpinning vascular smooth muscle tone. Biochem. Pharmacol. 203, 115205 https://doi.org/10.1016/j.bcp.2022.115205.

Berendsen, H.J.C., van der Spoel, D., van Drunen, R., 1995. GROMACS: a message-passing parallel molecular dynamics implementation. Comput. Phys. Commun. 91, 43–56. https://doi.org/10.1016/0010-4655(95)00042-E.

Budriesi, R., Cosimelli, B., Ioan, P., Ugenti, M.P., Carosati, E., Frosini, M., Fusi, F., Spisani, R., Saponara, S., Cruciani, G., Novellino, E., Spinelli, D., Chiarini, A., 2009. L-Type calcium channel blockers: from diltiazem to 1,2,4-oxadiazol-5-ones via thiazinooxadiazol-3-one derivatives. J. Med. Chem. 52 (8), 2352–2362. https://doi.org/10.1021/jm801351u.

Carullo, G., Ahmed, A., Trezza, A., Spiga, O., Brizzi, A., Saponara, S., Fusi, F., Aiello, F., 2020. Design, synthesis and pharmacological evaluation of ester-based quercetin derivatives as selective vascular $K_{Ca}1.1$ channel stimulators. Bioorg. Chem. 105, 104404 https://doi.org/10.1016/j.bioorg.2020.104404.

Chen, C., Gao, J.L., Liu, M.Y., Li, S.L., Xuan, X.C., Zhang, X.Z., Zhang, X.Y., Wei, Y.Y., Zhen, C.L., Jin, J., Shen, X., Dong, D.L., 2017. Mitochondrial fission inhibitors suppress endothelin-1-induced artery constriction. Cell. Physiol. Biochem. 42 (5), 1802–1811. https://doi.org/10.1159/000479536.

Cuong, N.M., Khanh, P.N., Duc, H.V., Huong, T.T., Tai, B.H., Binh, N.Q., Durante, M., Fusi, F., 2014. Vasorelaxing activity of two coumarins from *Murraya paniculata* leaves. Biol. Pharm. Bull. 37 (4), 694–697. https://doi.org/10.1248/bpb.b13-00905.

Fusi, F., Durante, M., Sgaragli, G., Khanh, P.N., Son, N.T., Huong, T.T., Huong, V.N., Cuong, N.M., 2015. *In vitro* vasoactivity of zerumbone from *Zingiber zerumbet*. Planta Med. 81, 298–304. https://doi.org/10.1055/s-0034-1396307.

Fusi, F., Durante, M., Spiga, O., Trezza, A., Frosini, M., Floriddia, E., Teodori, E., Dei, S., Saponara, S., 2016. *In vitro* and *in silico* analysis of the vascular effects of asymmetrical N,N-bis(alkanol)amine aryl esters, novel multidrug resistance-reverting agents. Naunyn-Schmiedeberg's Arch. Pharmacol. 389 (9), 1033–1043. https://doi.org/10.1007/s00210-016-1266-y.

Fusi, F., Ferrara, A., Zalatnai, A., Molnar, J., Sgaragli, G., Saponara, S., 2008. Vascular activity of two silicon compounds, ALIS 409 and ALIS 421, novel multidrug-resistance reverting agents in cancer cells. Cancer Chemother. Pharmacol. 61 (3), 443–451. https://doi.org/10.1007/s00280-007-0488-6.

Fusi, F., Marazova, K., Pessina, F., Gorelli, B., Valoti, M., Frosini, M., Sgaragli, G., 2000. On the mechanisms of the antispasmodic action of some hindered phenols in rat aorta rings. Eur. J. Pharmacol. 394 (1), 109–115. https://doi.org/10.1016/s0014-2999(00)00152-7.

Fusi, F., Saponara, S., Frosini, M., Gorelli, B., Sgaragli, G., 2003. L-type Ca^{2+} channels activation and contraction elicited by myricetin on vascular smooth muscles. Naunyn-Schmiedeberg's Arch. Pharmacol. 368 (6), 470–478. https://doi.org/10.1007/s00210-003-0836-y.

Fusi, F., Saponara, S., Sgaragli, G., Cargnelli, G., Bova, S., 2002. Ca(2+) entry blocking and contractility promoting actions of norbormide in single rat caudal artery myocytes. Br. J. Pharmacol. 137 (3), 323–328. https://doi.org/10.1038/sj.bjp.0704877.

Gessner, G., Cui, Y.M., Otani, Y., Ohwada, T., Soom, M., Hoshi, T., Heinemann, S.H., 2012. Molecular mechanism of pharmacological activation of BK channels. Proc. Natl. Acad. Sci. U. S. A. 109 (9), 3552–3557. https://doi.org/10.1073/pnas.1114321109.

Gurney, A.M., 1994. Mechanisms of drug-induced vasodilation. J. Pharm. Pharmacol. 46 (4), 242–251. https://doi.org/10.1111/j.2042-7158.1994.tb03789.x.

Hom, J., Yu, T., Yoon, Y., Porter, G., Sheu, S.S., 2010. Regulation of mitochondrial fission by intracellular Ca^{2+} in rat ventricular myocytes. Biochim. Biophys. Acta 1797 (6–7), 913–921. https://doi.org/10.1016/j.bbabio.2010.03.018.

Hom, J.R., Gewandter, J.S., Michael, L., Sheu, S.S., Yoon, Y., 2007. Thapsigargin induces biphasic fragmentation of mitochondria through calcium-mediated mitochondrial fission and apoptosis. J. Cell. Physiol. 212 (2), 498–508. https://doi.org/10.1002/jcp.21051.

Hoppins, S., Lackner, L.L., Lee, J.E., Mears, J.A., 2020. *In vitro* and *in vivo* assays for mitochondrial fission and fusion. Methods Cell Biol. 155, 491–518. https://doi.org/10.1016/bs.mcb.2019.11.010.

Iozzi, D., Schubert, R., Kalenchuk, V.U., Neri, A., Sgaragli, G., Fusi, F., Saponara, S., 2013. Quercetin relaxes rat tail main artery partly via a PKG-mediated stimulation of $K_{Ca}1.1$ channels. Acta Physiol. 208 (4), 329–339. https://doi.org/10.1111/apha.12083.

Jesmin, S., Sakuma, I., Hattori, Y., Fujii, S., Kitabatake, A., 2002. Long-acting calcium channel blocker benidipine suppresses expression of angiogenic growth factors and prevents cardiac remodelling in a Type II diabetic rat model. Diabetologia 45 (3), 402–415. https://doi.org/10.1007/s00125-001-0765-6.

Kim, S., Chen, J., Cheng, T., Gindulyte, A., He, J., He, S., Li, Q., Shoemaker, B.A., Thiessen, P.A., Yu, B., Zaslavsky, L., Zhang, J., Bolton, E.E., 2019. PubChem 2019 update: improved access to chemical data. Nucleic Acids Res. 47 (D1), D1102–D1109. https://doi.org/10.1093/nar/gky1033.

Koebel, M.R., Schmadeke, G., Posner, R.G., Sirimulla, S., 2016. AutoDock VinaXB: implementation of XBSF, new empirical halogen bond scoring function, into AutoDock Vina. J. Cheminform. 8, 27. https://doi.org/10.1186/s13321-016-0139-1.

Lackner, L.L., Nunnari, J., 2010. Small molecule inhibitors of mitochondrial division: tools that translate basic biological research into medicine. Chem. Biol. 17 (6), 578–583. https://doi.org/10.1016/j.chembiol.2010.05.016.

Lisowski, P., Kannan, P., Mlody, B., Prigione, A., 2018. Mitochondria and the dynamic control of stem cell homeostasis. EMBO Rep. 19 (5), e45432 https://doi.org/10.15252/embr.201745432.

Liu, M.Y., Jin, J., Li, S.L., Yan, J., Zhen, C.L., Gao, J.L., Zhang, Y.H., Zhang, Y.Q., Shen, X., Zhang, L.S., Wei, Y.Y., Zhao, Y., Wang, C.G., Bai, Y.L., Dong, D.L., 2016. Mitochondrial fission of smooth muscle cells is involved in artery constriction. Hypertension 68 (5), 1245–1254. https://doi.org/10.1161/HYPERTENSIONAHA.116.07974.

Macia, E., Ehrlich, M., Massol, R., Boucrot, E., Brunner, C., Kirchhausen, T., 2006. Dynasore, a cell-permeable inhibitor of dynamin. Dev. Cell 10 (6), 839–850. https://doi.org/10.1016/j.devcel.2006.04.002.

Maneechote, C., Palee, S., Chattipakorn, S.C., Chattipakorn, N., 2017. Roles of mitochondrial dynamics modulators in cardiac ischaemia/reperfusion injury. J. Cell Mol. Med. 21 (11), 2643–2653. https://doi.org/10.1111/jcmm.13330.

McCluskey, A., Daniel, J.A., Hadzic, G., Chau, N., Clayton, E.L., Mariana, A., Whiting, A., Gorgani, N.N., Lloyd, J., Quan, A., Moshkanbaryans, L., Krishnan, S., Perera, S., Chircop, M., von Kleist, L., McGeachie, A.B., Howes, M.T., Parton, R.G., Campbell, M., Sakoff, J.A., Wang, X., Sun, J.Y., Robertson, M.J., Deane, F.M., Nguyen, T.H., Meunier, F.A., Cousin, M.A., Robinson, P.J., 2013. Building a better dynasore: the dyngo compounds potently inhibit dynamin and endocytosis. Traffic 14 (12), 1272–1289. https://doi.org/10.1111/tra.12119.

McDonald, T.F., Pelzer, S., Trautwein, W., Pelzer, D.J., 1994. Regulation and modulation of calcium channels in cardiac, skeletal, and smooth muscle cells. Physiol. Rev. 74 (2), 365–507. https://doi.org/10.1152/physrev.1994.74.2.365.

Morris, G.M., Huey, R., Lindstrom, W., Sanner, M.F., Belew, R.K., Goodsell, D.S., Olson, A.J., 2009. AutoDock 4 and AutoDockTools 4: automated docking with selective receptor flexibility. J. Comput. Chem. 30 (16), 2785–2791. https://doi.org/10.1002/jcc.21256.

Mugnai, P., Durante, M., Sgaragli, G., Saponara, S., Paliuri, G., Bova, S., Fusi, F., 2014. L-type Ca(2+) channel current characteristics are preserved in rat tail artery myocytes after one-day storage. Acta Physiol. 211 (2), 334–345. https://doi.org/10.1111/apha.12282.

O'Boyle, N.M., Banck, M., James, C.A., Morley, C., Vandermeersch, T., Hutchison, G.R., 2011. Open Babel: an open chemical toolbox. J. Cheminform. 3, 33. https://doi.org/10.1186/1758-2946-3-33.

Park, R.J., Shen, H., Liu, L., Liu, X., Ferguson, S.M., De Camilli, P., 2013. Dynamin triple knockout cells reveal off target effects of commonly used dynamin inhibitors. J. Cell Sci. 126 (Pt 22), 5305–5312. https://doi.org/10.1242/jcs.138578.

Pergel, E., Veres, I., Csigi, G.I., Czirják, G., 2021. Translocation of TMEM175 lysosomal potassium channel to the plasma membrane by dynasore compounds. Int. J. Mol. Sci. 22 (19), 10515 https://doi.org/10.3390/ijms221910515.

Persaud, A., Cormerais, Y., Pouyssegur, J., Rotin, D., 2018. Dynamin inhibitors block activation of mTORC1 by amino acids independently of dynamin. J. Cell Sci. 131 (1), jcs211755 https://doi.org/10.1242/jcs.211755.

Pettersen, E.F., Goddard, T.D., Huang, C.C., Couch, G.S., Greenblatt, D.M., Meng, E.C., Ferrin, T.E., 2004. UCSF Chimera–a visualization system for exploratory research and analysis. J. Comput. Chem. 25 (13), 1605–1612. https://doi.org/10.1002/jcc.20084.

Ramachandran, R., 2018. Mitochondrial dynamics: the dynamin superfamily and execution by collusion. Semin. Cell Dev. Biol. 76, 201–212. https://doi.org/10.1016/j.semcdb.2017.07.039.

Reddy, P.H., 2014. Inhibitors of mitochondrial fission as a therapeutic strategy for diseases with oxidative stress and mitochondrial dysfunction. J. Alzheimers Dis. 40 (2), 245–256. https://doi.org/10.3233/JAD-132060.

Rovira-Llopis, S., Bañuls, C., Diaz-Morales, N., Hernandez-Mijares, A., Rocha, M., Victor, V.M., 2017. Mitochondrial dynamics in type 2 diabetes: pathophysiological implications. Redox Biol. 11, 637–645. https://doi.org/10.1016/j.redox.2017.01.013.

Salentin, S., Schreiber, S., Haupt, V.J., Adasme, M.F., Schroeder, M., 2015. PLIP: fully automated protein-ligand interaction profiler. Nucleic Acids Res. 43 (W1), W443–W447. https://doi.org/10.1093/nar/gkv315.

Saponara, S., Sgaragli, G., Fusi, F., 2008. Quercetin antagonism of Bay K 8644 effects on rat tail artery L-type Ca(2+) channels. Eur. J. Pharmacol. 598 (1–3), 75–80. https://doi.org/10.1016/j.ejphar.2008.08.016.

Saponara, S., Sgaragli, G., Fusi, F., 2002. Quercetin as a novel activator of L-type Ca(2+) channels in rat tail artery smooth muscle cells. Br. J. Pharmacol. 135 (7), 1819–1827. https://doi.org/10.1038/sj.bjp.0704631.

Saponara, S., Testai, L., Iozzi, D., Martinotti, E., Martelli, A., Chericoni, S., Sgaragli, G., Fusi, F., Calderone, V., 2006. (+/-)-Naringenin as large conductance Ca(2+)-activated K^+ (BK_{Ca}) channel opener in vascular smooth muscle cells. Br. J. Pharmacol. 149 (8), 1013–1021. https://doi.org/10.1038/sj.bjp.0706951.

Simonovic, N., Jakovljevic, V., Jeremic, J., Finderle, Z., Srejovic, I., Nikolic Turnic, T., Milosavljevic, I., Zivkovic, V., 2019. Comparative effects of calcium and potassium channel modulators on ischemia/reperfusion injury in the isolated rat heart. Mol. Cell. Biochem. 450 (1–2), 175–185. https://doi.org/10.1007/s11010-018-3384-y.

Teodori, E., Contino, M., Riganti, C., Bartolucci, G., Braconi, L., Manetti, D., Romanelli, M.N., Trezza, A., Athanasios, A., Spiga, O., Perrone, M.G., Giampietro, R., Gazzano, E., Salerno, M., Colabufo, N.A., Dei, S., 2019. Design, synthesis and biological evaluation of stereo- and regioisomers of amino aryl esters as multidrug resistance (MDR) reversers. Eur. J. Med. Chem. 182, 111655 https://doi.org/10.1016/j.ejmech.2019.111655.

Trezza, A., Spiga, O., Mugnai, P., Saponara, S., Sgaragli, G., Fusi, F., 2022. Functional, electrophysiology, and molecular dynamics analysis of quercetin-induced contraction of rat vascular musculature. Eur. J. Pharmacol. 918, 174778 https://doi.org/10.1016/j.ejphar.2022.174778.

Tykocki, N.R., Boerman, E.M., Jackson, W.F., 2017. Smooth muscle ion channels and regulation of vascular tone in resistance arteries and arterioles. Compr. Physiol. 7 (2), 485–581. https://doi.org/10.1002/cphy.c160011.

Vezzani, A., Wu, H.Q., Stasi, M.A., Angelico, P., Samanin, R., 1988. Effect of various calcium channel blockers on three different models of limbic seizures in rats. Neuropharmacology 27 (5), 451–458. https://doi.org/10.1016/0028-3908(88)90126-8.

Zhao, Y., Huang, G., Wu, J., Wu, Q., Gao, S., Yan, Z., Lei, J., Yan, N., 2019. Molecular basis for ligand modulation of a mammalian voltage-gated Ca^{2+} channel. Cell 177 (6). https://doi.org/10.1016/j.cell.2019.04.043, 1495-506.e12.